J. Biomed. Eng. Res : 107-113, 2008

Rotating-Gantry-Based X-Ray Micro-Tomography System with the Sliding Mechanism Capable of Zoom-In Imaging

Min Hyoung Cho, Dong Hun Lee, Byung Hee Han, Soo Yeol Lee

Department of Biomedical Engineering, Kyung Hee University
(Received November 5, 2007. Accepted December 11, 2007)

Abstract

We introduce a rotating-gantry-based x-ray micro-tomography system to be used for small animal imaging studies. It has the zoom-in imaging capability for high resolution imaging of a local region inside the animal subject without any contrast anomalies arising from truncation of the projection data. With the sliding mechanism mounted on the rotating gantry holding the x-ray source and the x-ray detector, we can control the magnification ratio of the x-ray projection data. By combining the projection data from the large field of view (FOV) scan of the whole animal subject and the projection data from the small FOV scan of the region of interest, we can obtain artifact-free zoomed-in images of the region of interest. For the acquisition of x-ray projection data, we use a 1248×1248 flat-panel x-ray detector with the pixel pitch of 100 mm. It has been experimentally found that the developed system has the spatial resolution of up to 12 lp/mm when the highest magnification ratio of 5:1 is applied to the zoom-in imaging. We present some *in vivo* rat femur images to demonstrate utility of the developed system for small animal imaging.

Key words : micro-tomography, zoom-in imaging, small animal imaging, rotating gantry, flat panel detector

Ⅰ. INTRODUCTION

Micro-tomography, often called micro-CT, is one of the small animal imaging modalities which can be used for longitudinal imaging studies of laboratory animals raised with disease developments or genetic manipulations [1-3]. It is of paramount importance to screen laboratory animals in a minimally invasive way using micro-CT since longitudinal observations through the lifetime of animal subjects are essential in many kinds of studies such as investigation of new drug effect with human disease models [4-7]. For the accurate measurement of organ anatomy in a minimally invasive way, micron-resolution imaging capability of micro-CT has been greatly utilized in high resolution imaging of complex-structured tissues such as trabecular bones [8,9] and micro vessels [10].

In order to take whole-body trans-axial images of a live animal using a micro-CT, the field of view (FOV) of the micro-CT should be bigger than the width of the animal subject. Recent micro-CT developments with a flat-panel detector [11, 12] or optic-taper-coupled multiple CCDs [13] have made it possible to scan the whole body of an animal as large as an adult rat. In whole body imaging with a large FOV, it is inevitable to increase the pixel resolution. To obtain high resolution images of a region of interest (ROI) in the animal subject, the zoom-in micro-tomography technique has been introduced [14]. In the zoom-in micro-tomography, two kinds of projection data sets are acquired, one from the large FOV scanning of the whole body and the other from the small FOV scanning of the ROI. The large FOV projection data are, then, used to substitute the missing projection data outside the FOV in the limited FOV projection data. Using the zoom-in micro-tomography technique, *in vivo* rat femur imaging has been successfully performed for longitudinal observation of trabecular thickness changes in Sprague-Dawley (*SD*) rats raised with the osteoporosis model [9].

In small animal imaging *in vivo* using a micro-CT, it is desirable to scan the animal subjects while they are lying in a natural posture on the couch. By doing so, we can reduce fitful motions of the animal subjects under anesthetization during the scan, thereby, reducing the motion artifacts in the reconstructed images. We have often observed violent fitful motions

This study was supported by a grant of the Korea Health 21 R&D Project, Ministry of Health and Welfare (02-PJ3-PG6-EV07-0002) and a grant from the Korea Science and Engineering Foundation (R11-2002-103).
Corresponding Author : Soo Yeol Lee, Professor
Department of Biomedical Engineering Kyung Hee University
1 Seochun, Kiheung, Yongin, Kyungki 446-701 Korea
Tel : +82-31-201-2980 / Fax : +82-31-201-3666
E-mail : sylee01@khu.ac.kr

of the anesthetized animal subjects while they are being tightly fixed to the supporter in upright posture during the scan in an object-rotating type micro-CT system. For the mitigation of this trouble, several commercial micro-CTs having the rotating gantry structure have been introduced. However, they have no flexibility in controlling the spatial resolution since they are based on the fixed-magnification-ratio imaging. In this study, we introduce a rotating-gantry-based x-ray micro-CT system which is capable of high-resolution zoom-in imaging of a small region inside the animal subject. The rotating gantry is capable of changing the magnification ratio of the x-ray imaging, and a 1248×1248 flat panel x-ray detector is used for the acquisition of 2-dimensional (2D) projection data. Performances of the developed micro-CT are presented along with some bony tissue images of live rats.

II. MATERIALS AND METHODS

A. The Rotating Gantry for Zoom-In Micro-Tomography

For zoom-in micro-tomography, we need to acquire two kinds of projection data sets, one from the full FOV scanning of the whole body of the animal subject and the other from the limited FOV scanning of a ROI inside the subject [14]. The limited FOV scanning is targeted to the ROI inside the subject with a larger magnification than the full FOV scanning. Even though the limited FOV projection data has better spatial resolution than the full FOV projection data, artifact-free images cannot be reconstructed from the limited FOV projection data due to their incompleteness, i.e., truncation of the projection data outside the FOV. In zoom-in micro-tomography, the missing projection data outside the FOV is estimated from the full FOV projection data. Once the missing projection data has been calculated from the full FOV projection data, the calculated projection data outside the FOV is augmented to the limited FOV projection data to reconstruct artifact-free images of the ROI.

In the previous study of zoom-in micro-tomography [14], the animal subject had been tied to the rotation stage for the scan just like a conventional x-ray micro-CT. To change the magnification ratio of the x-ray projection data, the rotation stage was moved along the sliding mechanism with the x-ray source and the x-ray detector fixed at a predetermined position. In this study, we have made a rotating gantry on which a sliding mechanism is mounted as shown in Fig. 1. The rotating gantry is made of a circular aluminum plate with the diameter and thickness of 540mm and 20mm, respectively. The sliding mechanism, depicted as the linear motion (LM) actuator with the aluminum mount on it and the size of 85×65×570 mm^3, is mounted on the rotating gantry (Fig. 2). The LM actuator is driven by a servo motor through a ball screw with the pitch of 3 mm. The angular resolution of the servo motor is 0.036° which makes the sliding precision be ±0.3 μm. The rotating gantry is driven by another servo motor with the angular resolution of 0.036°. The servo motor is coupled with the rotating gantry through a 100:1 speed reduction gear. With the speed reduction gear, the rotational motion of the rotating gantry can be controlled with the angular resolution of 3.6 $\times 10^{-4}$ °. The rotating gantry weighs about 35 kg with all the other parts, i.e., the x-ray source, the x-ray detector and the sliding mechanism, mounted on it. Several weight balancers are applied on the rotating gantry to secure constant angular speed of the gantry during the scan. The gantry-driving servo motor has the maximum torque of 3.8 Nm. The rotation speed can be controlled from 1.5 min to 30 min per rotation. Since

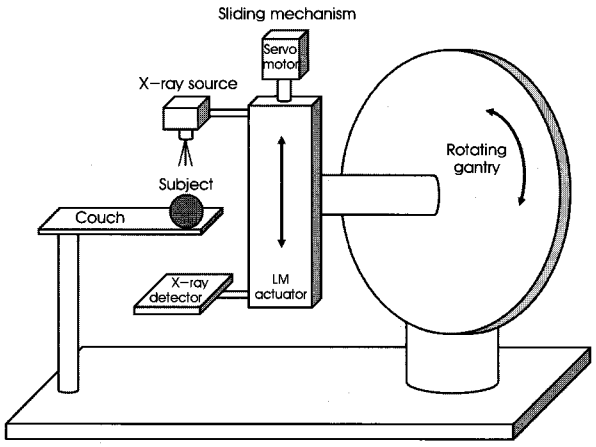

Fig. 1. The schematic diagram of the rotating gantry micro-tomography system with the sliding mechanism. On the sliding mechanism, an x-ray source and a flat-panel x-ray detector are mounted.

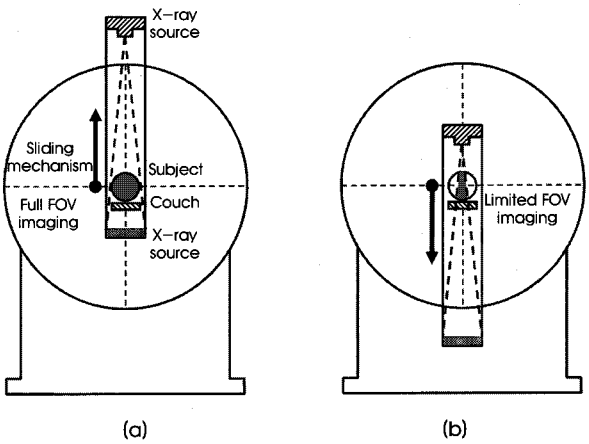

Fig. 2. The relative position of the x-ray source and the x-ray detector (a) in the full FOV scan and (b) in the limited FOV scan.

one rotation suffices for a3-dimensional imaging with a flat-panel detector, flexible cables are used for all the elec- trical wirings between the system controller and the rotating gantry without using slip rings.

The x-ray source and the x-ray detector are fixed on the aluminum mount which is movable along the ball screw in the sliding mechanism. The relative positions of the x-ray source and the x-ray detector with respect to the rotational center are controlled by sliding mechanism as shown in Fig. 2. The x-ray source to detector distance, *SD*, has been set to 456 mm, and the x-ray source to the animal subject distance, *SO*, has been controlled between 91 mm and 380 mm, which makes the magnification ratio vary from 1.2:1 to 5.0:1.

B. The X-Ray Source and the X-Ray Detector

To improve signal-to-noise ratio (SNR) in live animal imaging, we used amicro-focus x-ray source (5000Apogee, Oxford Instruments, USA) which has a rather large nominal focal spot size of 35 μm. The x-ray tube is a sealed tube with a fixed tungsten anode having an angle of 11° against the electron beam and with a 127 μm-thick beryllium exit window. The emitted x-ray beam angle is about 22°. The maximumtube voltage and tube current are 50 kV and 1 mA, respectively. The micro-focus x-ray source has been operated in a continuous mode with an Al filter with the thickness of 1mm.

We used a commercially available flat-panel detector (C794 3SPL, Hamamatsu, Japan) to acquire 2D x-ray projection data. The flat-panel detector consists of a 1248×1248 active matrix of transistors and photodiodes with a pixel pitch of 100 μm, and a CsI:Tl scintillator. The sensitive area of the detector is about 12×12 cm^2 which is large enough to cover an adult *SD* rat. The optical photons, emitted from CsI:Tl when irradiated by x-rays, have a peak spectrum at about 560 nm (or ~2.2 eV in equivalent energy), and they are converted to electrical charges in the readout photodiode array. The pixel fill factor is 80% in spite of the small pixel size of 100 μm. The CsI:Tl has a columnar structure with a typical diameter of about 10 μm and the thickness of 200 μm.

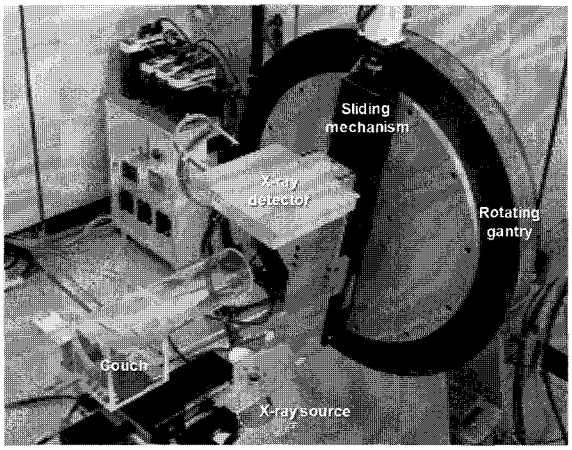

Fig. 3. A photograph of the developed micro-tomography system

C. Phantom and Animal Imaging

After fabricating the micro-CT as shown in Fig. 3, we have evaluated spatial resolution and contrast-to-noise performance of the developed micro-CT. For the spatial resolution measurements, we took cross-sectional images of a thin gold wire which has the diameter of 20 μm. We set *SD* and *SO* to 456 mm and 380 mm, respectively, in the full FOV imaging, and we changed *SO* to 120 mm in the limited FOV imaging. Hence, the magnification ratios were 1.2:1 and 3.8:1 in the full FOV imaging and in the limited FOV imaging, respectively. We applied the tube voltage and current of 40 kVp and 0.55 mA, respectively, with the presumed focal spot size of 35 μm. The number of views was 450 over 360° and the detector frame time was 2.0 s both in the full FOV imaging and in the limited FOV imaging. After obtaining cross-sectional gold wire image $g(x, y)$, we calculated one-dimensional Fourier transform, $G(k_x)$, of the centre profile of the gold wire image, i.e., $g(x, 0)$. To take into account the nonzero-width effect of the gold wire on the modulation transfer function (MTF), we divided $G(k_x)$ by the Fourier transform of the profile function of the gold wire. The dividend, then, represents the MTF of the micro-CT.

Table 1. The density and pixel values of the regions in the contrast phantom image.

Regions	Material	Density (g/cm3)	Pixel values (mean ± standard deviation)	
			Full FOV imaging	Zoom-in imaging
A	Acrylic	1.18	5.09±0.225	5.19±0.611
B	Polystyrene	1.11	4.13±0.242	4.12±0.613
C	Polycarbonate	1.18	5.03±0.249	4.97±0.642
D	Plastic water	1.03	8.03±0.237	8.21±0.686
E	Nylon	1.15	4.97±0.207	4.99±0.624
F	Polyethylene	0.95	3.94±0.244	3.94±0.618

We have tested low-contrast visibility of the zoom-in imaging using a contrast phantom whose photograph and tomographic images are shown in Fig. 6. The contrast phantom consists of six inserts whose physical densities are similar to that of water. The insert pointed by the arrow is plastic water, and the others are nylon, polyethylene, acryl, polystyrene and polycarbonate clockwise from the plastic water. The inserts were made of commercial electron density phantoms (Model 76-430, Nuclear Associates, NY, USA). Physical properties of the six inserts are shown in Table 1. The six inserts with the diameter of 5 mm are immersed in the cylindrical acryl water bath with the diameter of 40 mm. For the evaluation of the spatial resolution, we placed an electrolytic capacitor (22 μF, 25V) with the diameter and length of 5 mm and 11 mm, respectively, in the center of the phantom. We applied the tube voltage of 40 kVp and current of 0.55 mA for the contrast phantom imaging with the presumed focal spot size of 35 μm. All the other imaging parameters are the same as in the spatial resolution measurement.

In vivo small animal imaging has been performed with an adult *SD* rat weighing 400 g. The *in vivo* animal imaging has been performed at 40 kVp and 0.55 mA with all the imaging parameters kept the same as in the contrast phantom imaging. During the scan, the rat was anesthetized with combination of 1.5% isoflurane (Choong-Wae Pharma Co., Korea), 70% N_2O and 30% O_2 gas, and the anesthetizing gas was delivered with a gas anesthesia machine (Tabletop research anesthesia machine sets, SurgiVet, USA).

D. Image Reconstruction

In the image reconstruction, 3D whole body images are firstly reconstructed from the full FOV projection data set using the Feldkamp algorithm [15]. Before applying the 3D reconstruction algorithm, we applied flat field correction and dead pixel/line correction to the acquired 2D projection data. We used linear interpolation for the dead pixel/line correction. After reconstructing the full FOV 3D images (Fig. 4(a)), we calculated the missing projection data outside the FOV in the limited FOV scan as shown in Fig. 4(b). The missing projection data in the region II has been calculated by ray-tracing the full FOV 3D images. We scaled the calculated projection data so that the two projection data sets, one acquired by the flat-panel detector in region I and the other calculated in region II, are continuous at the interface between the two regions. After augmenting the calculated projection data to the acquired projection data, we reconstructed 3D images of the ROI using the Feldkamp algorithm.

For fast image reconstruction, we used the parallel image processing system. To realize a parallel image processing system for the 3D image reconstruction, we have linked four personal computers, each one equipped with dual CPUs (Athlon MP 2200+, AMD, USA), with 100 Mbps Ethernet and assigned evenly divided tasks to each of the eight CPUs. One of the four computers is chosen as a host computer and the host computer controls the whole micro-CT system.

III. RESULTS

The MTF measurement results are showed in Fig. 5. The MTFs of the full FOV imaging and the zoom-in imaging are shown as circles and squares, respectively. If we assume that the limiting spatial resolution corresponds to the point when the MTF drops to 10%, we can infer that the spatial resolution limits of the micro-tomography system are about 12 lp/mm

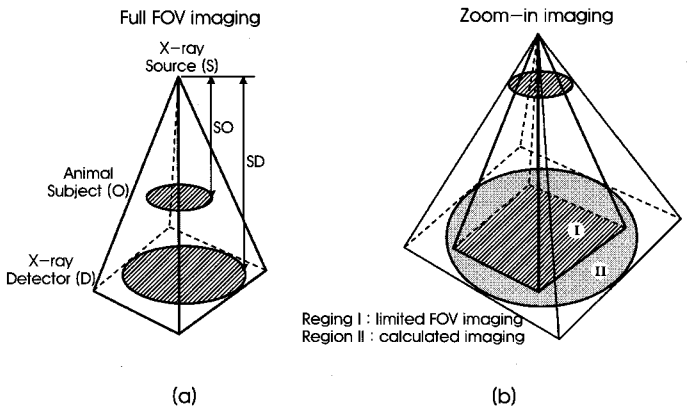

Fig. 4. The projection data on the flat panel detector (a) in the full FOV imaging and (b) in the zoom-in imaging. The missing projection data outside the detector (region II) is calculated from the full FOV projection data.

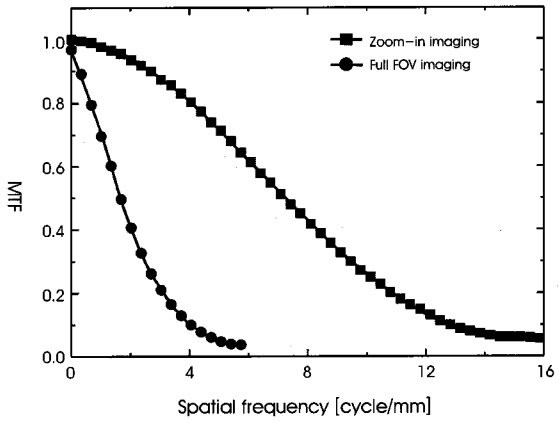

Fig. 5. Measured MTFs of the micro-tomography system. The MTFs of the full FOV imaging and the zoom-in imaging are shown as circles and squares, respectively.

and 4 lp/mm in the zoom-in imaging and the full FOV imaging, respectively. The spatial resolution improvement in zoom-in imaging is about 3. Since the magnification ratio of the zoom-in imaging is about 3.8times bigger than the full FOV imaging, the maximal improvement in the spatial resolution should be about 3.8 times. The smaller improvement in the spatial resolution is thought to be mainly due to the non-zero focal spot size of the x-ray tube.

Figure 6(a) shows a photograph of the contrast phantom consisting of six inserts and an electrolytic capacitor in the center. In Fig. 6(b), (c), and (d), we have shown the cross-sectional image of the contrast phantom obtained from the full FOV imaging, the magnified image obtained by applying bilinear interpolation to Fig. 6(b),and the zoom-in micro-tomography image, respectively. The spatial resolution of the full FOV imaging and the zoom-in imaging are 83 μm and 26 μm isometric resolution. As can be noticed from Fig. 6(b), three of the inserts are clearly differentiated from the background water, and the rest of them are barely differentiated. However, the internal structure of the electrolytic capacitor cannot be seen in Fig. 6(c) dueto the poor spatial resolution. In Fig. 6(d), the spiral electrodes in the capacitor can be clearly seen owing to its improved spatial resolution. In Fig. 6(c), we have shown the magnified image of Fig. 6(b). Figure 6(c) has been obtained by applying bilinear interpolation to Fig. 6(b). The pixel mean values and standard deviations at the six insert regions are shown in Table 1. As can be noticed from Table 1, the contrast values in the zoomed-in image are very similar to the ones in the full FOV image. The noises, i.e., standard deviations, in the zoomed-in images are about 2.5 ~ 3 times bigger than they are in the full FOV image. Since SNR of a CT image is inversely proportional to $\triangle x\sqrt{H}$ ($\triangle x$: pixel size, H: detector slice thickness) if the system noise is neglected [16], the degree of SNR degradation of the zoomed-in images could be as big as 2.4 times. The little more SNR degradation than the expectation is due to the stronger ring artifacts in the zoom-in imaging.

The cross-sectional images of a live adult *SD* rat are shown in Fig. 7. Figure 7(a) and (b) show a full FOV image and its magnified image in the femur bone region. Due to the limited spatial resolution, the trabecular bone structure is not clearly seen in Fig. 4(b). Figure 4(c) shows the ROI (the circled region) image obtained with the zoom-in micro-tomography technique. Owing to its better spatial resolution, the visibility of the trabecular bone structure is now much improved in Fig. 4(c).

Ⅳ. DISCUSSIONS AND CONCLUSIONS

We have introduced a rotating-gantry-based zoom-in micro-tomography system for small animal imaging. The rotating-gantry-based micro-CT imaging has many advantages over a conventional micro-CT imaging in which the animal subject is rotated during the conventional tomographic scan. By rotating

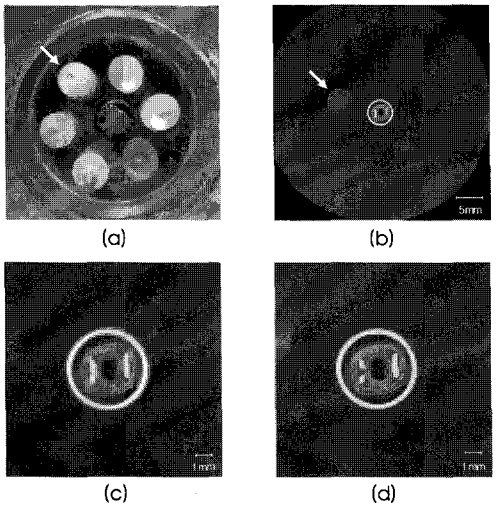

Fig. 6. (a) A photograph of the contrast phantomconsisting of six inserts and an electrolytic capacitor in the center. The insert pointed by the arrow is plastic water, and the others are nylon, polyethylene, acryl, polystyrene and polycarbonate clockwise from the plastic water. (b) A full FOV image of the phantom. (c) The magnified image obtained by applying bilinear interpolation to (b). (d) The zoom-in micro-tomography image of the phantom.

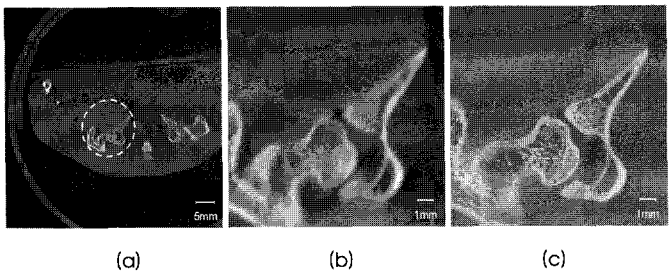

Fig. 7. (a) A full FOV image of a rat. (b) The magnified image obtained by applying bilinear interpolation to (a). (c) The zoom-in micro-tomography image of the circled region.

the x-ray source and x-ray detector pair for the scan while the animal subject lying in a natural posture, we can be freed from many problems related with rotating the animal subject. With the rotating-gantry-based micro-CT, we expect less motion artifacts in the reconstructed images, bigger survival rate of the animal subjects during the studies with anesthetization and shorter preparation time for the scan. The animal subject lying in a natural posture also allows physiological monitoring like ECG more easily.

Unlike the commercial rotating-gantry-based micro-CT system, the developed micro-CT system has the sliding mechanism on the rotating gantry for the zoom-in imaging. Thezoom-in imaging allows us high spatial-resolution imaging of a small region when the whole body imaging does not provide enough spatial resolution. Bony tissue imaging for osteoporosis studies and micro vessel imaging for angiogenesis studies [6,17] seem to be promising application areas. Micro imaging of bony tissues makes it possible to measure many kinds of parameters regarding trabecular bones. Convention micro tomographic imaging of bone samples has provided information to calculate trabecular thickness, bone-tissue volume ratio, bone surface-volume ratio, and trabecular number [18]. Recently, trabecular thickness measurement has been tried on live rats with the zoom-in micro-tomography technique [9]. With rat models having ovariectomy-induced osteoporosis, they successfully observed thinning process of the trabecular bones over several weeks without sacrificing them. We used the x-ray tube having rather large focal spot size to secure proper x-ray exposure level. To obtain better spatial resolution on the order of micron, an x-ray tube having smaller focal spot size may be used. But, it should be verified that the mechanical precision of the rotating gantry is good enough not to lose the benefit of the smaller focal spot size.

Motion artifacts are still great nuisances in small animal imaging with micro-CTs. Unlike human scans with clinical x-ray CTs, micro-CT images have poor SNR due to the much smaller pixel size and much lower exposure level than clinical scans. It seems that soft tissue visibility in small animal studies with a micro-CT cannot be ensured with a scan time shorter than a respiration period of small animals whatever detector types are used. Motion artifacts in zoom-in micro-tomography should be investigated in the future imaging studies of live small animals.

In conclusion, a rotating-gantry-based zoom-in micro-tomography system has been developed with a flat panel xray detector and a micro-focus x-ray source for localized imaging of a live small animal subject. It is expected that the proposed system can be greatly used for many kinds of in vivo small animal imaging studies.

REFERENCES

[1] M.G. Pomper, "Molecular imaging: an overview," *Acad. Radiol.*, vol. 8, pp. 1141-1153, 2001.

[2] R. Weissleder, and U. Mahmood, "Molecular imaging," *Radiology*, vol. 219, pp. 316-333, 2001.

[3] T.F. Massoud, and S.S. Gambhir, "Molecular imaging in living subject: seeing fundamental biological processes in a new light," *Genes & Development*, vol. 17, pp. 545-580, 2003.

[4] M.J. Paulus, H. Sari-Sarraf, S.S. Gleason, M. Bobrek, J.S. Hicks, D.K. Johnson, J.K. Behel, L.H. Thompson, and W.C. Allen, "A new x-ray computed tomography system for laboratory mouse imaging," *IEEE. Trans. Nucl. Sci.*, vol. 46, pp. 558-564, 1999.

[5] M.J. Paulus, S.S. Gleason, H. Sari-Sarraf, D.K. Johnson, C.J. Foltz, D.W. Austin, M.E. Easterly, E.J. Michaud, M.S. Dhar, P.R. Hunsicker, J.W. Wall, and M. Schell, "High-resolution x-ray CT screening of mutant mouse models," in *Proc. SPIE, San Jose*, CA, USA, Jan, 2000, vol. 3291, pp. 270-279.

[6] S.Y. Wan, A.P. Kiraly, E.L. Ritman, and W.E. Higgins," Extraction of the hepatic vasculature in rats using 3-D micro-CT images," *IEEE. Trans. Med. Imag.*, vol. 19, pp. 964-971, 2000.

[7] E.L. Ritman,"Molecular imaging in small animals-roles for micro-CT," *J. Cell. Biochem. Supp.*, vol. 39, pp. 116-124, 2002.

[8] R.D. Kapadia, G.B. Stroup, A.M. Badger, B. Koller, J.M. Levin, R.W. Coatney, R.A. Dodds, X. Liang, M.W. Lark, and M. Gowen, "Application of micro-CT and MR microscopy to study pre-clinical models of osteoporosis and osteoarthritis," *Technol. Health Care*, vol. 6, pp. 361-372, 1998.

[9] I.K. Chun, M.H. Cho, J.H. Park, and S.Y. Lee, "*In vivo* trabecular thickness measurement in cancellous bones: longitudinal rat imaging studies," *Physio. Meas.*, vol. 27, pp. 695-702, 2006.

[10] S.M. Jorgensen, O. Demirkaya, and E.L. Ritman, "Three-dimensional imaging of vasculature and parenchyma in intact rodent organs with x-ray micro-CT," *Am. J. Physiol.*, vol. 275, pp. H1103-1114, 1998.

[11] D.A. Jaffray, and J.H. Siewerdsen, "Cone-beam computed tomography with a flat-panel imager: initial performance characterization," *Med. Phys.*, vol. 27, pp. 1311-1123, 2000.

[12] S.C. Lee, H.K. Kim, I.K. Chun, M.H. Cho, S.Y. Lee, and M.H. Cho, "A flat-panel detector based micro-CT system: performance evaluation for small-animal imaging," *Phys. Med. Biol.*, vol. 48, pp. 4173-4185, 2003.

[13] W.C. Phillips, M. Stanton, A. Stewart, H. Qian, C. Ingersoll, and R.M. Sweet, "Multiple CCD detector for macromolecular x-ray crystallography," *J. Appl. Cryst.*, vol. 33, pp. 243-251, 2000.

[14] I.K. Chun, M.H. Cho, S.C. Lee, M.H. Cho, and S.Y. Lee, "X-ray micro-tomography system for small-animal imaging with zoom-in imaging capability," *Phys. Med. Biol.*, vol. 49, pp. 3889-3902, 2004.

[15] L.A. Feldkamp, L.C. Davis, and J.W. Kress, "Practical cone-beam algorithm," *J. Opt Soc. Am. A*, vol. 1, pp. 612-619, 1984.

[16] D.W. Holdsworth, M. Drangova, and A. Fenster, "A high-resolution XRII-based quantitative volume CT scanner," *Med. Phys.*, vol. 20, pp. 449-462, 1993.

[17] S.Y. Wan, E.L. Ritman, and W.E. Higgins, "Multi-generational analysis and visualization of the vascular tree in 3D micro-CT images," *Comput. Biol. Med.*, vol. 32, pp. 55-71. 2002.

[18] A.A. Kurth, and R. Muller, "The effect of an osteolytic tumor on the three-dimensional trabecular bone morphology in an animal model," *Skeletal Radiol.*, vol. 30, pp. 94-98, 2001.